Physica Medica 104 (2022) 101–111

Contents lists available at ScienceDirect

Physica Medica

journal homepage: www.elsevier.com/locate/ejmp

Ultra-high dose rate dosimetry for pre-clinical experiments with mm-small proton fields

M. Togno [a,*], K.P. Nesteruk [b], R. Schäfer [a], S. Psoroulas [a], D. Meer [a], M. Grossmann [a], J.B. Christensen [c], E.G. Yukihara [c], A.J. Lomax [a,d], D.C. Weber [a,e,f], S. Safai [a]

[a] Center for Proton Therapy, Paul Scherrer Institut, Villigen, Switzerland
[b] Department of Radiation Oncology, Massachusetts General Hospital and Harvard Medical School, Boston, USA
[c] Department of Radiation Safety and Security, Paul Scherrer Institut, Villigen, Switzerland
[d] Department of Physics, ETH Zurich, Zurich, Switzerland
[e] Department of Radiation Oncology, University Hospital Zurich, Zurich, Switzerland
[f] Department of Radiation Oncology, Inselspital, Bern University Hospital, University of Bern, Switzerland

A B S T R A C T

Purpose: To characterize an experimental setup for ultra-high dose rate (UHDR) proton irradiations, and to address the challenges of dosimetry in millimetre-small pencil proton beams.

Methods: At the PSI Gantry 1, high-energy transmission pencil beams can be delivered to biological samples and detectors up to a maximum local dose rate of ~9000 Gy/s. In the presented setup, a Faraday cup is used to measure the delivered number of protons up to ultra-high dose rates. The response of transmission ion-chambers, as well as of different field detectors, was characterized over a wide range of dose rates using the Faraday cup as reference.

Results: The reproducibility of the delivered proton charge was better than 1 % in the proposed experimental setup. EBT3 films, Al_2O_3:C optically stimulated luminescence detectors and a PTW microDiamond were used to validate the predicted dose. Transmission ionization chambers showed significant volume ion-recombination (>30 % in the tested conditions) which can be parametrized as a function of the maximum proton current density. Over the considered range, EBT3 films, inorganic scintillator-based screens and the PTW microDiamond were demonstrated to be dose rate independent within ±3 %, ±1.8 % and ±1 %, respectively.

Conclusions: Faraday cups are versatile dosimetry instruments that can be used for dose estimation, field detector characterization and on-line dose verification for pre-clinical experiments in UHDR proton pencil beams. Among the tested detectors, the commercial PTW microDiamond was found to be a suitable option to measure real time the dosimetric properties of narrow pencil proton beams for dose rates up to 2.2 kGy/s.

1. Introduction

Radiation therapy with ultra-high dose rates (UHDR) has gained momentum in recent years not only because of the beneficial impact on treatments' duration, but particularly for the promising reduction of adverse side effects to healthy tissue as observed in in-vivo experiments [1–4]. This so-called FLASH effect has been mainly investigated in electron beams [5,6], but pre-clinical studies in X-ray photons [7] as well as in proton and heavy-ion beams [8–10] are increasing in number. Whilst the biological mechanisms behind the FLASH effect are not yet fully understood, and more experiments are required to confirm the protecting effect in proton beams [11], several technical and metrological challenges arise in this unconventional irradiation modality [12]. Current dosimetry protocols are not designed for UHDR regime [13–15] as well as typical detectors used in clinics start to deviate from their expected behaviour when dose rate is increased beyond the conventional range [16,17]. Consequently, increasing efforts are being pursued to overcome the shortage of suitable dosimeters for the UHDR regime [18–20].

We present a methodology to perform accurate dosimetry in UHDR millimetre-small proton beams. Under these conditions, dose rate as well as volume averaging may affect dosimetry with conventional detectors (e.g. ion-chambers). Our approach relies on the use of a Faraday cup (FC) as a reference dose rate independent device [21]. Similar approaches making use of FC have been recently reported [8,22]. In the presented setup, FC reading, beam spread and integral depth-dose (IDD) curves are used to model the delivered dose. Moreover, the FC is used for on-line verification of the delivered dose, as well as to characterize the response of different field and monitor detectors up to UHDR. Field dosimeters under test were a synthetic single-crystal microDiamond

* Corresponding author.
E-mail address: michele.togno@psi.ch (M. Togno).

https://doi.org/10.1016/j.ejmp.2022.10.019
Received 7 May 2022; Received in revised form 10 October 2022; Accepted 23 October 2022
Available online 14 November 2022

TM60019 (PTW, Freiburg, Germany), EBT3 Gafchromic™ films (Ashland, Bridgewater, US) and a Gd_dO_2S:Tb scintillating screen coupled to a low-noise CCD camera (hereafter called 'CCD-system'). Whilst the microDiamond TM60019 has been extensively tested in UHDR pulsed electron beams [17,23] and in conventional proton beams [24–27], to the best of our knowledge it has never been tested in proton beam at dose rates exceeding 80 Gy/s [9]. Thanks to its properties (small sensitive volume, energy independence [24]) the microDiamond can potentially be used to perform real-time dosimetric measurements in millimetre-small UHDR proton beams.

Despite the challenging readout procedure, EBT3 films are still considered a reliable dosimetry system especially for dosimetry in small fields. They have been proven to be dose rate independent in electron beams up to 8×10^6 Gy/s [28,29] and only recently characterized in proton beams up to 7.5 kGy/s [30]. In the present work, we have extended the investigated dose rate range up to 9 kGy/s.

Inorganic scintillators coupled with cameras or photomultipliers have been largely used in conventional radiotherapy [31–33]. Their application to the UHDR regime has been limited so far and to our knowledge to relative [9,11] or time resolved [34,35] measurements. In our study, we aimed at testing the dose rate response of an in-house developed system based on Gd_dO_2S:Tb scintillator up to 2220 Gy/s.

For the validation of the estimated dose, we also made use of Al_2O_3:C optically stimulated luminescence dosimeters (OSLDs) which have been previously characterized in our experimental setup with UHDR proton beams [36].

The presented experiments were performed at the PSI Gantry 1, which was the first gantry in the world to deliver pencil beam scanning (PBS) proton therapy to cancer patients [37]. After the clinical operations ceased at the end of 2018, the system was turned into an experimental platform to study the effects of UHDR high energy proton beams [38]. As such, Gantry 1 and the proposed setup can nowadays be used to run pre-clinical experiments with biological samples to explore the potential FLASH effect of proton beams, as well as to characterize the response of a dosimetry apparatus when exposed to ultra-high dose rates.

2. Materials and methods

2.1. Experimental setup at PSI Gantry 1

The Gantry 1 beamline has been optimized to transport the undegraded 250 MeV proton beam extracted from the COMET accelerator to the treatment room [38]. After such optimization, the maximum beam transmission to the room isocenter was measured to be as high as (86±1) %, thus resulting in a maximum beam current in the treatment area of 690 nA. In what follows and unless otherwise specified, we always refer to the proton current in the treatment area. In addition, the

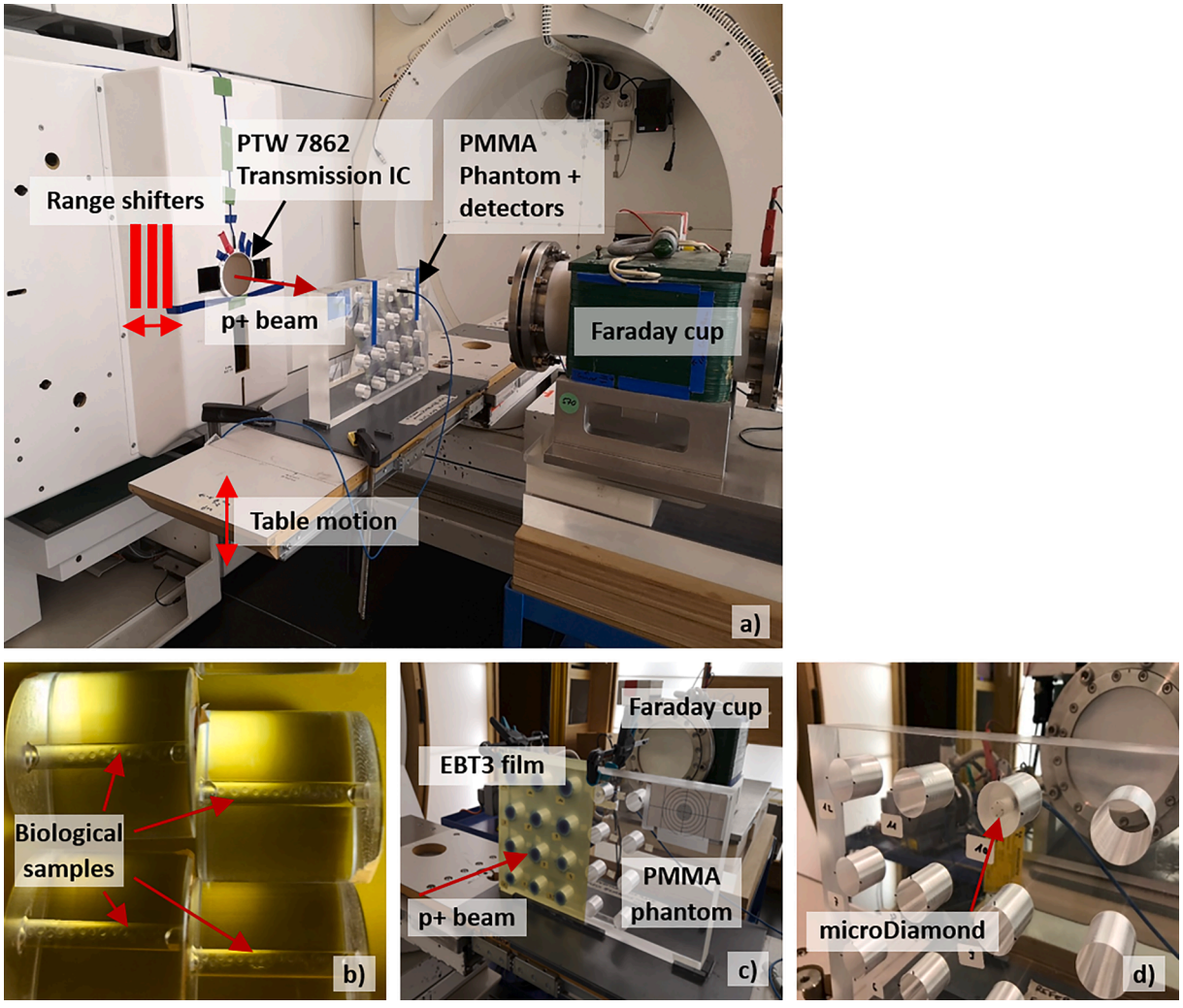

Fig. 1. a) Gantry 1 irradiation area. The Faraday cup is used as reference detector as well as beam dump. b) Hollow PMMA cylinders with Zebrafish embryos in water-based solution. c) PMMA phantom placed onto the movable table, with EBT3 film at the phantom surface. d) microDiamond detector inserted into the PMMA phantom.

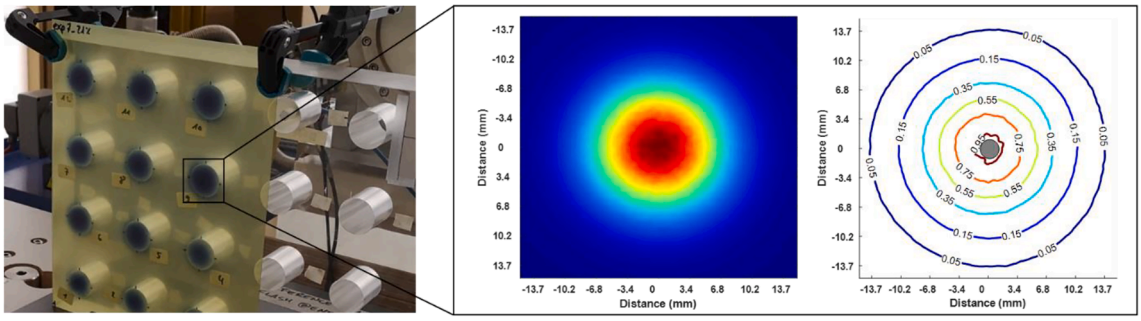

Fig. 2. Illustration of the single spot dose distribution (color washed) centered on the PMMA cylinder with a central hole of 2.5 mm diameter. The 95 % isodose level is defined to include an additional margin for alignment uncertainties.

Gantry 1 nozzle is equipped with 40 polystyrene (PS) plates, each plate of 4.53 mm physical thickness, which can be inserted into the beam path to degrade the beam energy and increase the downstream beam dimensions. When all the plates are inserted into the beam path, the beam energy is lowered to a minimum of about 170 MeV. Upstream of the range shifter plates, an air-vented plane-parallel ionization chamber (IC) is used to control the delivered dose [39]. This transmission chamber (Monitor 1) is biased with 2000 V and has an ion collection time of about 90 μs. Due to the much higher instantaneous dose rates achieved in our experiments compared to the clinical conditions, the response of Monitor 1 was characterized up to 690 nA proton current as discussed in Section 2.3. Magnetic scanning of the pencil proton beam can be realized in one transverse direction [38], but it has not been applied yet in pre-clinical experiments and therefore not further discussed in this work. The Gantry 1 irradiation area and experimental setup are shown in Fig. 1a.

In pre-clinical experiments [40], biological targets such as Zebrafish embryos were irradiated with single-spot transmission beams. The samples were located in a 2.5 mm hole drilled through the axis of a 2 cm long cylinder made of Poly Methyl Methacrylate (PMMA) (Fig. 1b). A PMMA phantom allocates multiple cylinders and gives the possibility to place build-up inserts of different thickness upstream of the cell lines. The phantom is fixed onto an experimental table, which can be driven remotely along three axis. Fig. 1c shows the PMMA phantom together with irradiated EBT3 films, in the setup as used for the biology experiments. Downstream of the PMMA phantom, a Faraday Cup [39] measures the transmission proton charge for each delivery. The FC is by design dose-rate independent, and it has been recently proposed as a practical tool for reference measurements in ultra-high dose rate proton beams [21]. As such, it can be used to quantify and monitor on-line the delivered number of protons (and therefore the delivered dose) to each biological sample, at different dose rates.

In addition to the FC and the built-in nozzle monitor IC, a transmission chamber type TM7862 (PTW, Freiburg, Germany) was used as a redundant monitor. Similar to any gas-filled ICs, the TM7862 chamber suffers of volume ion-recombination when irradiated with high dose rate beams. Its response had to be characterized against the FC, in a similar fashion as for Monitor 1, as reported in Section 2.3.

To ensure the pencil beam is properly steered to the PMMA cylinder axis, and therefore centered to the biological targets or any detector to be tested, the following procedure was implemented: first, the PTW microDiamond is inserted to the PMMA phantom by means of a dedicated holder (Fig. 1d), with its entrance window orthogonal to the beam direction and its axis coincident with the PMMA cylinder axis. The sensitive area (1.1 mm radius) of the microDiamond is similar to the hole's cross-section (1.25 mm radius) where the targets are deposited. The microDiamond is then aligned to the nozzle cross-hair lasers. Afterwards, a proton pencil beam is delivered and steered magnetically in the horizontal and vertical direction, in sub-millimetre steps. The signal measured by the microDiamond provides the convolution of the pencil beam with the detector sensitive area. Finally, the pencil beam position is set in such a way that the reading of the detector is at its maximum.

To ensure a uniform dose coverage to the biological samples, in our experiments the proton pencil beam in air is modified by inserting PS plates in the nozzle so that the samples lie completely within the 95 % isodose level (Fig. 2). An additional safety margin of 0.25 mm is considered for possible alignment errors. Concurrently, the samples are distributed, along the beam direction, at a water equivalent depth that ranges between 25.7 mm and 45.7 mm. For a given energy of the protons impinging on the phantom of about 244.4 MeV, this ensures the samples to be irradiated uniformly in depth with the highest achievable dose rate.

For a fixed configuration (number) of PS plates inserted into the beam path, the dose rate can be adjusted by varying the proton current in the treatment area. Since the beam extracted from the COMET cyclotron is quasi-continuous (pulse repetition frequency PRF = 72.85 MHz), the dose rate is defined, here and throughout the manuscript, as the average dose rate during the irradiation of each spot, i.e. the delivered dose divided by the irradiation time t as measured by the control system. In a similar way the proton current i_p is defined as the ratio of the proton charge Q_{FC} measured in air by the FC divided by the irradiation time t, i.e, $i_p = Q_{FC}/t$. The actual proton current, and in turns the dose rate, in a single 0.8 ns long beam pulse is 17.5 times higher than under the assumption of continuous beam, at the same time the dose in the pulse is extremely low. This and other quantities of interest are further detailed in Section 2.2.

2.2. Pencil beam dose model

To control the dose delivered in our experiments, a calibration of the primary monitor in terms of Monitor Units per deposited dose (MU/Gy) is required. While the calibration of Monitor 1 in terms of MU per delivered proton (MU/p) is straightforward with a FC [41] and has already been described elsewhere for our experimental setup [38], the quantity Gy/p is estimated through a simple analytical model, as detailed in the following. We describe the dose $D(x,y,z)$ at the point of interest (x,y,z) within the proton pencil beam by a double Gaussian beam model:

$$D(x,y,z) \cong \left(-\frac{1}{\rho}\frac{dE}{dz}(E_0)\right)_w \cdot \frac{Q_{FC}}{e} \cdot IDD_R(z) \cdot \frac{1}{2\pi\sigma_x(z)\sigma_y(z)} \cdot \exp\left(-\left(\frac{(x-x_0)^2}{2\sigma_x^2(z)} + \frac{(y-y_0)^2}{2\sigma_y^2(z)}\right)\right) \quad 2.1$$

where z describes the direction along the beam axis (i.e. the depth in the dosimetry phantom), x and y define the plane orthogonal to the beam axis and E_0 is the residual energy of the incident protons at the surface of the phantom.

The ratio Q_{FC}/e represents the total number of protons n_p impinging on the dosimetry phantom (for the dose model, Q_{FC} is measured without the phantom in the beam path, whereas for online measurements a phantom attenuation factor is determined). $(-\frac{1}{\rho}\frac{dE}{dz}(E_0))_w$ is the mass stopping power in water for protons of energy E_0. A large plane-parallel ionization chamber type TM34070 (PTW, Freiburg, Germany) in a motorized water tank was used to measure the integral depth dose (IDD) curve for the pristine beam with mean initial energy E_0. In our model, IDD_R is the measured integral depth dose curve normalized to its value at the phantom entrance, i.e. $IDD_R(z) = IDD(z)/IDD(z=0)$.

The last term in equation (2.1) is the normalized Gaussian distribution that describes the lateral spread of the proton beam when travelling through the phantom. Clearly, the local dose, and therefore the local dose rate, is maximum on the pencil beam axis, i.e. when $x = x_0$ and $y = y_0$, and it scales quadratically with the spread magnitude.

The root-mean-square (rms) widths of the Gaussian distribution, σ_x and σ_y, at a specific depth z are determined as:

$$\sigma_{x,y}(z)^2 = (\sigma_{x,y}(z)^2)_{optics} + (\sigma_{x,y}(z)^2)_{MCS} \quad 2.2$$

The first term $(\sigma_{x,y}(z)^2)_{optics}$ is calculated from the parametrization of the in air spatial-angular distribution, i.e. the phase space, of the proton beam, following the generalized Fermi-Eyges solution to the diffusion equation [42]. In practice, the phase space is determined by means of spot size measurements via scintillating screen viewed by a CCD camera [43] placed at varying distances from the nozzle.

The term $(\sigma_{x,y}(z)^2)_{MCS}$ describes the gain in the distribution width due to the Multiple Coulomb Scattering (MCS) of protons diffusing in the medium. In our case, we consider MCS in the phantom only, as the contribution from the air upstream the phantom, as well as from the range shifter plates, is already parametrized in $(\sigma_{x,y}(z)^2)_{optics}$. Following the work of Safai et al. [42] the MCS contribution from the phantom is calculated through the Highland's parametrization of the transport equation, with Lynch and Dahl constants [44].

Naturally, the distribution widths σ_x and σ_y depend on the depth z, on the beam energy as well as on the initial spatial distribution, and therefore different phase-space parametrizations are needed for different initial energies E_0 and different range shifter plates' configuration.

In our model, we assume the width of the distribution to be independent of the beam current, therefore implying the maximum dose rate on the beam axis to change linearly with the beam current. In practice, small but significant deviations can occur, as detailed in the Discussion section.

Fig. 3 illustrates, as an example, the beam spatial spread for two different beam configurations used in our study, along with the resulting dose rate distributions on the beam axis, for a beam current of 520 nA, in an ideal water phantom. The beam configuration A.2 consists of a pencil beam with initial spatial spread at the nozzle exit of 0.32 cm (contribution from the optics and 3 PS plates in the nozzle) and energy E_0 of 244.4 MeV. The beam configuration B.1 results from different settings of the optics and has an initial spatial spread of 0.16 cm and energy E_0 of 250 MeV. These and other quantities of interest for different beam configurations are summarized in Table 1.

The overall uncertainty associated to the pencil beam dose model was estimated to be of the order of 5 %, combining the uncertainties on the delivered proton charge, on the measured IDD and on the beam spread. The dose estimated with the model was verified in the experimental setup described in section 2.1 and beam configuration A.2 – the same used for the biological experiments – with different detectors: a synthetic single-crystal microDiamond TM60019 (PTW, Freiburg, Germany), EBT3 Gafchromic™ films (Ashland, Bridgewater, US) and Al_2O_3:C OSLDs.

2.3. Dose rate response of large plane-parallel ion-chambers (i.e. monitors) using narrow pencil beams

To control the dose delivered to the biological samples within the desired accuracy, the Monitor 1 chamber response at different dose rates had to be characterized thoroughly. As a matter of fact, this chamber was originally designed to operate at beam currents 2 to 3 order of magnitude lower than those used in our experiments. The

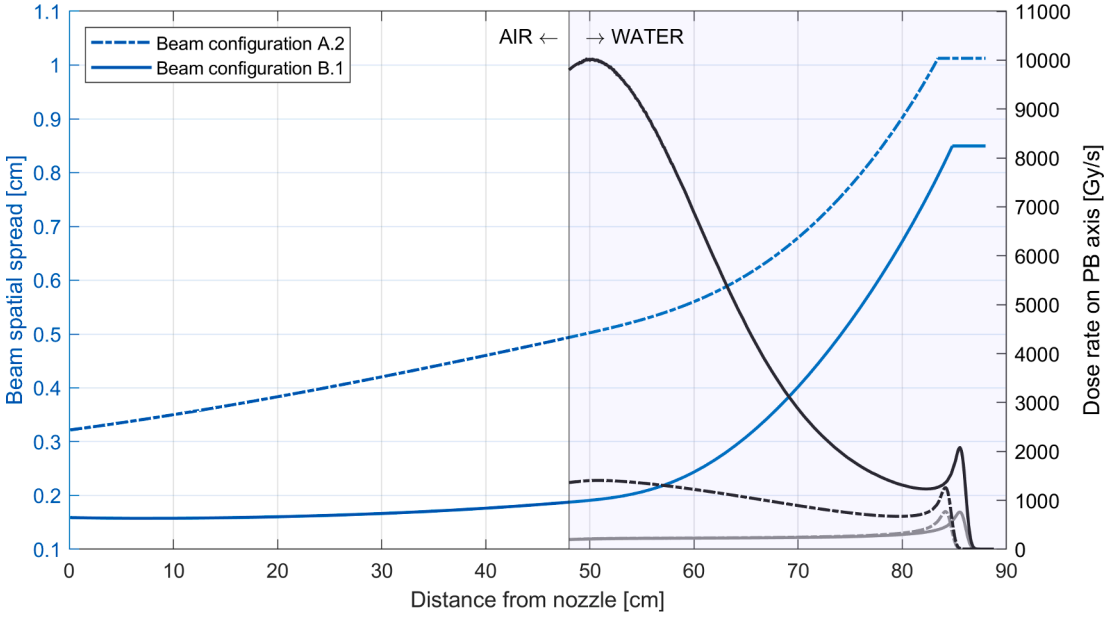

Fig. 3. Beam spatial spread and dose rate distribution along the beam axis for two different beam configurations (details about beam configurations in Table 1). The dose rate distributions are calculated for the same number of incident protons. The IDD curves are also displayed (light grey – not to scale) with illustrative purpose. The water surface starts at 48 cm distance from the nozzle.

Table 1
Beam configurations and relative beam parameters used in our studies. Pre-clinical experiments with biological specimens were performed with beam configuration A.2.

	Beam optics setting (tune)	PS plates (#)	Energy E_0 (MeV)	Beam σ at nozzle exit (mm)	Beam σ at phantom surface (mm)	Calculated max dose rate for 520nA beam current (Gy/s)
Beam configuration A.1	*A*	0	250	3.0	3.5	2780 ± 140
Beam configuration A.2	*A*	3	244.4	3.2	4.9	1400 ± 70
Beam configuration B.1	*B*	0	250	1.6	2.0	10020 ± 510
Beam configuration B.2	*B*	7	237.2	2.5	6.2	1050 ± 52

characterization of Monitor 1 has already been described in [38], hereafter we summarize the methodology and the results.

The electric field strength in the air cavity of Monitor 1 is equal to 400 kV/m (electrode spacing = 0.5 cm, chamber voltage = 2 kV, ion collection time = 90 μs). Therefore, a decrease in the ion-collection efficiency is expected due to the onset of volume recombination for large beam currents. To quantify the efficiency loss, the response of the chamber was compared to the response of the Faraday cup over a large span of beam currents (0.2–690) nA. The obtained calibration curve is then used to estimate the amount of Monitor Units (MU) required to deliver the desired number of protons to the dosimetry phantom. On the day of the experiment, the ratio MU/p is verified for two selected beam currents, as a sanity check of the calibration curve.

The same approach was used to characterize the response of the PTW TM7862 (S/N 521) which features an electrode spacing of 0.24 cm, 0.5 kV chamber voltage and ion collection time (t_c) of 80 μs. The chamber was attached to the nozzle exit as a redundant monitor. As such, this chamber is used to assess the delivered charge after each irradiation, rather than to control the delivery itself. Similar curves as for Monitor 1 were measured for the PTW TM7862 by means of the FC. The curves were fitted with two separate models, i.e. the model derived by Boag and Wilson [45] for recombination under continuous beams (the condition $\frac{1}{PRF} \ll t_c$ is satisfied, being the PRF equal to 72.85 MHz):

$$f = \frac{2}{1+\sqrt{1+\frac{2}{3}\xi^2}} \tag{2.3}$$

and a logistic model adapted from Petersson et al. [16]:

$$f = \frac{1}{(1+(\chi)^{\alpha})^{\beta}} \tag{2.4}$$

In Eqs. (2.3) and (2.4), both the term $\xi = md^2\sqrt{q}V$ and $\chi = V/q$ depend on the ionization density q within the chamber air cavity. The other quantities m, d and V are parameters that include the recombination coefficient and the ionic mobility, the distance between IC electrodes, and the IC voltage, respectively.

In addition, the stability of the chamber response over time was assessed for high (~520 nA) and low (~0.38 nA) beam currents.

2.3.1. Characterization of the response as a function of the proton current density of narrow pencil beams

It should be noted that, for a given configuration of the beam optics (beam tune), the calibration of Monitor 1 in terms of MU/p at different beam currents is unique, while the calibration of the PTW TM7862 in terms of $Coulomb/p$ depends also on the PS plates inserted in the beam path. In fact, the more PS plates are inserted, the larger is the beam spatial spread in the chamber air cavity, which implies a decreased local dose rate (or ionization density) and a decreased volume recombination. In the following, we outline the method to generalize the response of large ionization chambers using narrow Gaussian pencil beams of variable spot size. We make the following assumptions:

- the charge collection efficiency of the plane-parallel ionization chamber is uniform across the plane of the chamber
- the maximum proton current density experienced by the chamber when delivering a narrow pencil beam is representative for the ion recombination effect in the chamber

Without loss of generality, let's assume that a Gaussian cylindrical symmetric pencil beam with rms (σ) transvers a large ionization chamber. The fluence $\Phi(r)$ across the chamber at a radial distance r from the axis of the incident pencil beam can be expressed with

$$\Phi(r) = \frac{n_p}{2\pi\sigma^2}\cdot\exp\left(-\frac{r^2}{2\sigma^2}\right) \tag{2.5}$$

where n_p is the total number of protons crossing the chamber as determined by the FC ($n_p = Q_{FC}/e$).

The proton current density distribution $j(r)$ can then be expressed with

$$j(r) = e\cdot\dot{\Phi}(r) = \frac{i_p}{2\pi\sigma^2}\cdot\exp\left(-\frac{r^2}{2\sigma^2}\right) \tag{2.6}$$

where $\dot{\Phi}$ is the particle flux (fluence rate) and i_p the proton current as defined earlier. Consequently the maximum proton current density j_{max} experienced by the chamber is

$$j_{max} = j(0) = \frac{i_p}{2\pi\sigma^2} \tag{2.7}$$

It is therefore expected that representing the dependency of the chamber response as a function of the maximum proton current density rather than i_p will make the behaviour independent from the beam size used to test the equipment.

Again, in this study i_p is determined via FC measurements in air, and σ via measurement with the CCD-system. In case of an asymmetric Gaussian pencil beam with different rms σ_x and σ_y, then σ should be replaced with the product $(\sigma_x\sigma_y)$ in the equation above.

2.4. Dose rate dependence of field detectors

We made use of the FC to characterize the response at different dose rates of different field detectors, specifically the aforementioned EBT3 Gafchromic™ films, microDiamond TM60019 (S/N P22197), and Gd_dO_2S:Tb based CCD-system.

2.4.1. EBT3 Gafchromic™ films

EBT3 films were irradiated with a single pencil beam with energy E_0 in the range (237.2–250) MeV, i.e. with all beam configurations from Table 1, at a water equivalent depth of 2.5 cm. The dose rate over the investigated range (1–9000) Gy/s is meant to be the maximum lateral dose rate $\dot{D}_{max}$ corresponding to the dose rate in the centre of the beam lateral Gaussian distribution. The maximum as well as the spread of the measured beam spot is extracted by fitting a bi-dimensional Gaussian function.

From Eq. (2.5), and given that the maximum dose D_{max} deposited by particles with the same energy is directly proportional to the maximum particle fluence, i.e. $D_{max} \propto \Phi_{max}$, we have

$$D_{max} \propto \frac{Q_{FC}}{\sigma_x \sigma_y} \quad 2.8$$

The measured maximum dose is therefore multiplied with the factor $(\sigma_x \sigma_y)/Q_{FC}$ to obtain a constant value. The factor accounts for different beam spread due to different beam tunes/PS configurations, and for possible differences in the total delivered protons.

EBT3 films were previously calibrated in absolute dose to water up to 20 Gy against an Advanced Markus TM34045 chamber (PTW, Freiburg, Germany). Dose calibration was performed at PSI Gantry 2, with both films and IC simultaneously irradiated in a PMMA phantom with a large uniform 230 MeV beam. The energy dependence of the films was checked in the (200–230) MeV range and found to be smaller than the measurement uncertainty. For both calibration and measurements, EBT3 films were readout with a flatbed scanner Epson 1000 XL and analysed with a Matlab® routine. Net optical density as well as its parametrization as function of dose were defined according to Devic et al. [46].

2.4.2. PTW microDiamond

Fig. 4 shows the experimental setup to test the dose rate response of the microDiamond detector. The detector was irradiated with a single pencil beam and beam configuration A.1. The diamond was inserted into a dedicated hollow PMMA cylinder which fits the dosimetry phantom, with the detector sensitive disc orthogonal to the beam propagation axis. The microDiamond was previously calibrated in absolute dose to water against a Farmer IC FC65-G (IBA Dosimetry GmbH, Schwarzenbruck, Germany): the microDiamond and the Farmer IC were irradiated with an homogeneous box of 2 Gy (modulation 10 cm, distal range 20 cm), in a water tank, at PSI Gantry 2. The energy/LET dependence of the microDiamond in proton beams has been previously investigated by Goma et al. [24] and found to be negligible.

The FC, placed downstream of the phantom, was used to normalize the detector reading. The CCD-system was installed upstream of the phantom to measure the spatial spread for each delivered beam. With this setup we were able to calculate corrections to estimate the true microDiamond response in the following way. The actual reading of the microDiamond S_D is proportional to the actual number of protons crossing the detector sensitive area, given by the integration of the particle fluence distribution $\Phi(r)$ over such area (with radius r_D), i.e.

$$S_D \propto \int_0^{2\pi} \int_0^{r_D} \Phi(r) r dr d\theta = \frac{Q_{FC}}{e} \cdot \left(1 - exp\left(-\frac{r_D^2}{2\sigma^2}\right)\right) \equiv \varepsilon \quad 2.9$$

As such the corrected reading S_D/ε allows to investigate the response by accounting for beam size fluctuations and variation in the delivered number of protons. In our study, in eq. (2.9), instead of σ we used the average sigma $\sqrt{\sigma_x \sigma_y}$.

2.4.3. Gd_dO_2S:Tb scintillating screen-CCD system

The data collected during the characterization of the microDiamond detector (Fig. 3), in particular the CCD images and the FC readings, allow to characterize the CCD-system response at different dose rates. A similar image-fitting process as described for EBT3 films was used to extract the desired quantities from the measured beam spots. As opposed to EBT3 films, no dose calibration is needed.

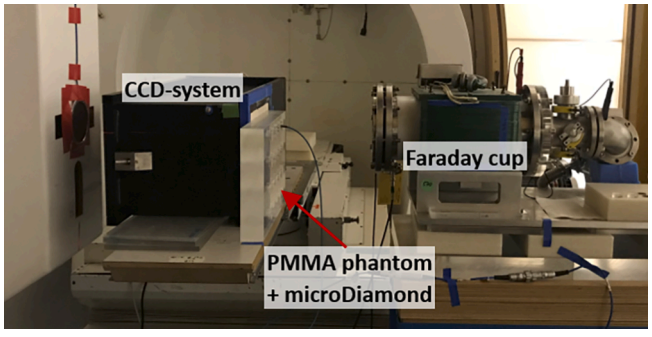

Fig. 4. CCD-system, PMMA phantom and microDiamond setup onto the movable table.

2.4.4. Al_2O_3:C OSLDs

The Al_2O_3:C OSLDs have been demonstrated to be dose rate independent in proton beams [36]. For the validation of the estimated dose from the model, the OSLDs were cut to a 2 mm diameter from a 47 μm thick sheet. The dose calibration, preparation, and readout procedures are described in [36]. Although the OSLDs are capable of simultaneous dose and LET measurements [47], which allows for ionization quenching corrections, no quenching corrections were applied to the doses due to the high proton energies with a negligible quenching.

3. Results

3.1. Pencil beam dose model validation

We present the results of the model validation for a selected dose of 10 Gy (target dose) with beam configuration A.2 as reported in Table 1. These results remain valid for any dose level, assuming the dose varies linearly with the number of protons (or MUs) for a given beam configuration and beam current.

EBT3 films, microDiamond and OSLDs were irradiated simultaneously, and the responses were corrected taking into account the relative effective depth of measurement. A dose rate correction (1.5 %) was also applied to the microDiamond response at 520 nA based on the results presented in section 3.3. The measured EBT3 dose distribution was averaged over the effective sensitive area of the microDiamond for a direct comparison. Due to their millimetre-large size, the OSLDs are assumed to provide already an averaged comparable signal.

Data presented in Fig. 5 are the mean values over six subsequent deliveries, and the error bars (k=1) combine the repeatability of the measurements with the uncertainties from alignment and dose cross-calibration factors. All three dosimeter types clearly measure a dose lower than the target.

When considering the average of the doses from the three dosimeters, the deviation from the target dose is −9 % and −8 % for low and high proton current, respectively. Noteworthy, the beam spread at 0.38nA was measured to be larger (+0.125 mm, +2.5 %) than the beam spread as calculated in the beam model. At the same time, the beam spread at 520 nA was measured to be smaller (−0.07 mm, −1.3 %) than the beam spread at 0.38 nA.

After correcting the target dose from the model with the actual values of the beam spread, the difference to the measured dose is then reduced to −2.9 % at 0.38 nA and to −4.1 % at 520 nA.

The difference in the beam spread between low and high proton current is a rather small but detectable effect that has been observed with a reproducible pattern with both EBT3 films and the CCD-system.

Based on microDiamond measurements, which have been demonstrated to be the more reproducible, the average dose rate delivered to the cells in the PMMA cylinders is estimated to be (0.90±0.04) Gy/s and (1260±50) Gy/s for 0.38 nA and 520 nA proton current, respectively.

3.2. Dose rate dependence of monitor ion-chambers

The measured Monitor 1 efficiency curve for beam tune A, normalized at 0.4 nA proton current, is shown in Fig. 6. The beam spatial spread is estimated to be about 0.27 cm in the chamber air cavity (the chamber is located about 50 cm upstream of the nozzle exit and 26 cm upstream of the last PS plate). We have identified three regions of the curve to be modelled with different functions: up to 8 nA proton current the efficiency is stable around 100 % and no corrections are introduced, from 8 nA up to 690 nA the efficiency drops to 82 % and the curve is fitted with

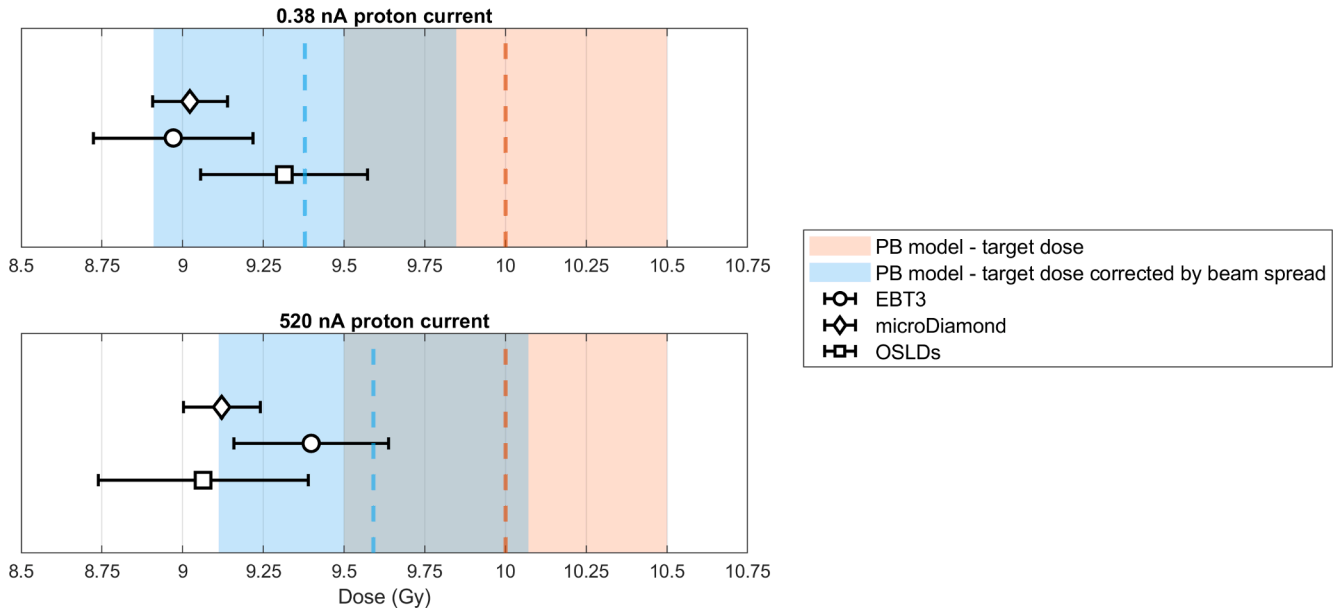

Fig. 5. Dose validation with beam configuration A.2 – also used for irradiation of cell lines in biological experiments. Beam parameters: 3 PS plates, $E_0 = 244.4$ MeV, proton current 0.38 nA and 520 nA, initial beam spread 0.32 cm, beam spread at the dosimeters location 0.505 cm.

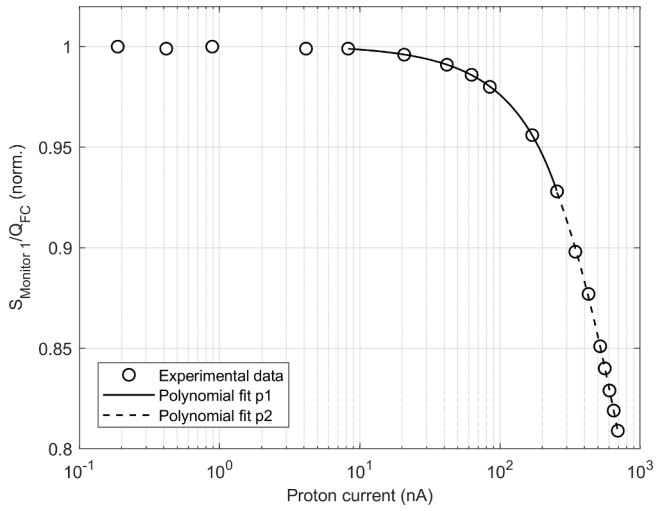

Fig. 6. Ratio of the signal from Monitor 1 ($S_{Monitor1}$) and the charge measured by the FC (Q_{FC}). Full ion-collection efficiency is assumed with bias of 2000 V at 0.4 nA, as found in Lin et al. [39]. The two polynomial fits 'p1' and 'p2' are quadratic functions of the proton current with R^2-value = 1.

two different polynomials to account for a change in concavity around 255 nA. As previously reported [38], with this calibration based on FC as reference detector we were able to reach an accuracy better than 1 % in the delivered proton charge, for all the explored dose rates.

For a given setting of the beam optics, different efficiency curves were measured with the PTW TM7862 chamber depending on the number of PS plates inserted upstream of the detector. Data acquired with two different beam configurations are reported in Fig. 7a, specifically:

- beam configuration B.1, proton current range (0.7–613) nA
- beam configuration B.2, proton current range (0.8–582) nA

The measured efficiency at the maximum proton current is 68 % and 80 % for beam configuration B.1 and B.2, respectively. The theoretical model from Boag (eq. (2.3)) poorly agrees with the data, especially when no PS plates are in place, with a R^2-value of the fit of 0.986. The logistic model described by the equation (2.4) provides a better fit to the experimental data, with R^2-value of 0.998 and 1 when no PS plates and 7 PS plates are in place, respectively.

As outlined in section 2.3.1, the response of the chamber can be modelled with a single function independently of the beam size when plotted against the maximum current density as shown in Fig. 7b. The logistic model fitted in Fig. 7b results in a R^2-value of 0.997.

The TM7862 chamber was found to be reproducible – over a period of 6 months – within ±0.5 % and within ±2 % for 0.38 nA and 520 nA, respectively.

3.3. Dose rate dependence of field detectors

The response of the microDiamond at different dose rates in the (0.3–2220) Gy/s range, normalized to the FC reading, is shown in Fig. 8. As presented in section 3.1, the beam spatial spread measured by the CCD-system was found to have a slight but non-negligible dependence on the dose rate, with a difference of 80 μm (2 %) between maximum and minimum dose rate in this specific setup. When the normalized data are not corrected for this variation in the beam size, the microDiamond response appears to increase with increasing dose rate. However, if the measured beam size is accounted for, the microDiamond response decreases with a logarithmic-like behaviour and reaches a maximum deviation of 2 % between maximum and minimum dose rate. Fig. 8 also shows the correction factor ε, normalized to the incident number of protons. As a consequence of the mentioned variation in the beam spread, the correction factor ε varies about 4 % over the investigated dose rate range.

Noteworthy, after correcting for the true beam size, the repeatability of the measurements is affected as follows:

- It is improved for measurements at dose rates $>10^3$ Gy/s (>300 nA proton current). In this range and for a fixed beam current, the beam size might undergo fluctuations with order of magnitude of tens of μm, which are significant compared to the uncertainty associated with the measurement of the beam size.
- It is worsened for measurements at dose rates $<10^3$ Gy/s (<300 nA proton current). In this range, the fluctuations of the beam size are

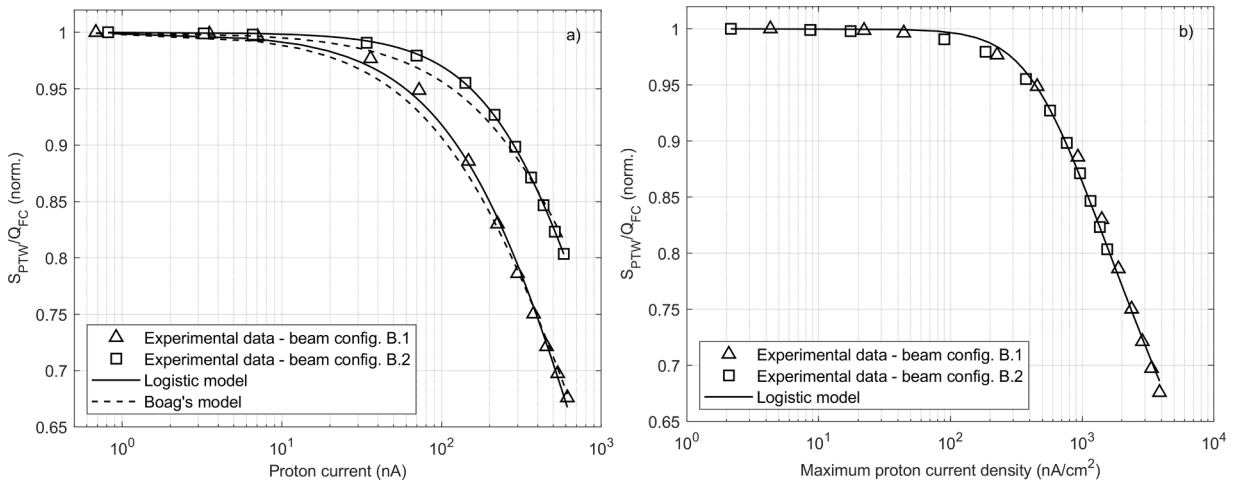

Fig. 7. a) Ratio of the signal from PTW TM7862 (S_{PTW}) and the charge measured by the FC (Q_{FC}). For both configurations, full collection efficiency is expected at the lowest measured proton current. b) Ratio S_{PTW}/Q_{FC} as function of the maximum current density (equation (2.7)).

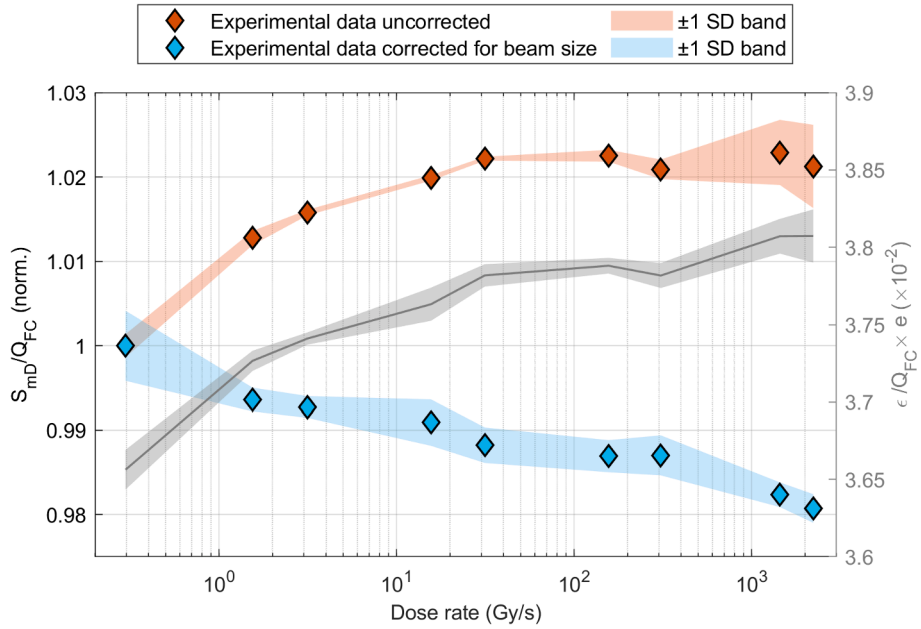

Fig. 8. The microDiamond response as function of the dose rate. The curves are normalized to the point at the lowest dose rate, i.e. 0.3 Gy/s.

even smaller and the repeatability of the corrected data is affected by the accuracy of the beam size measurements.

Fig. 9a and Fig. 9b illustrates the dose rate response of the EBT3 films and CCD-system, respectively. The data are normalized to the average response in the (1–10) Gy/s dose rate range. For EBT3 films, data are scattered around the average value with maximum deviations from the average within ±3 % (k=2). Within this band, a dose rate effect is not visible up to about 9 kGy/s. For the CCD-system, an increase of the response with the dose rate can be identified, even though the deviations from the average are within ±1.8 % (k=2). At present, we have not identified any possible undesired bias in our measurements and/or data analysis that could have affected the presented data.

4. Discussion

The mechanisms underlying the FLASH effect still require investigations. Being able to achieve precise dose delivery and dose verification is of paramount importance for such studies. In our work we address the dosimetric aspects of an irradiation setup which has been previously proven to achieve UHDR regime with proton beams [38].

The dose per delivered proton (Gy/p) at different depths and positions in a PMMA dosimetry phantom was predicted through a model which is based on different measured parameters of the proton pencil beam – the phase space, the IDD and the total number of protons. A major source of uncertainty in the predicted dose was identified to be the beam spatial spread. As mentioned in the results session, the size of the beam was found to slightly change between high and low proton currents, as well as between different measurement sessions. We have retrospectively analysed the data collected over one year of experiments with biological assays (Fig. 10), and found that the beam spread – measured in air at the entrance of the dosimetry phantom – shows variations up to ±0.15 mm (±3 %) compared to the value parametrized in the pencil beam model. Such variations are normally well within the tolerances for a clinical beam (±10 %) but can lead to a 6 % under(over)-estimation of the local dose on the beam axis. As demonstrated in section 3.1, the agreement between the model and the measured dose can be restored within uncertainties if the actual beam size is considered.

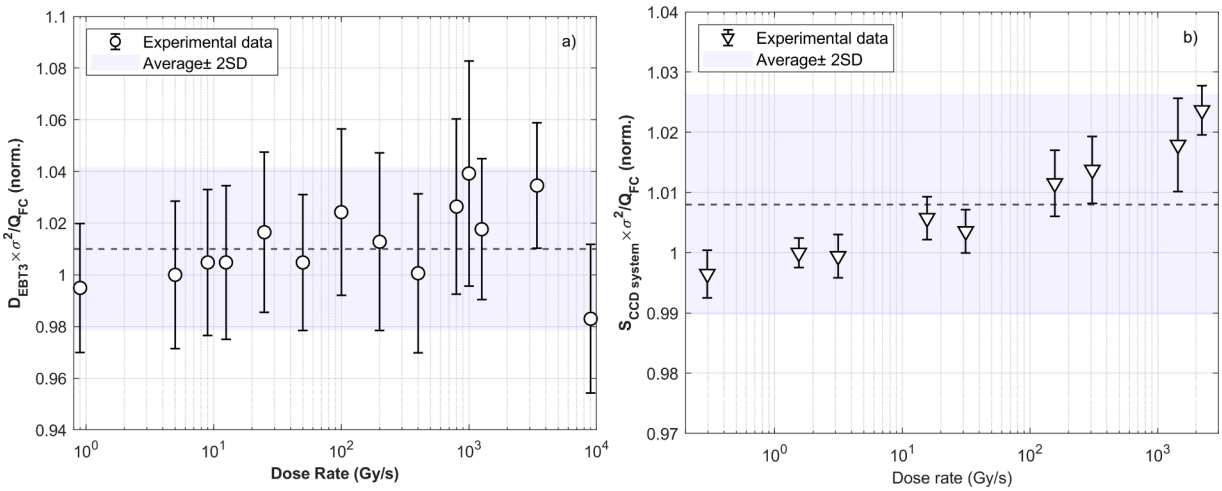

Fig. 9. a) EBT3 films and b) Gd_dO_2S:Tb scintillating screen response as a function of the dose rate. The dotted line indicates the average of the normalized data, while the coloured band represents the interval (average ±2 SD). EBT3 data were collected in both the experimental setups described in Christensen et al. [36].

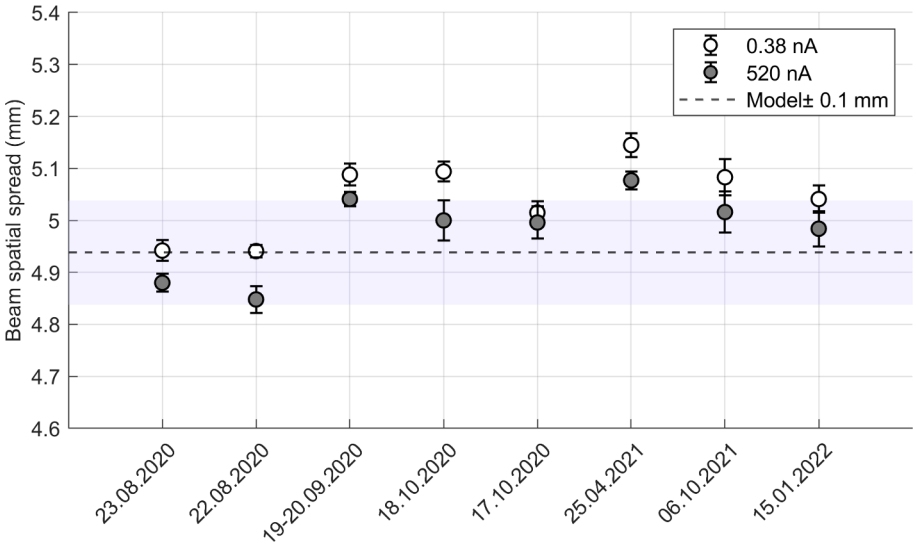

Fig. 10. Measured beam spatial spread – in air, at the entrance of PMMA phantom – in different experimental sessions. The date of measurements is reported on the horizontal axis.

The MCS contribution to the modelled beam width is calculated in water, and it does not consider hard scatters. The calculated MCS contribution to the total beam width is small in the first centimetres of the phantom and amounts to 0.11 mm and 0.27 mm at depths of 2.5 cm and 4.5 cm, i.e. where the biological samples and/or the dosimeters are placed. Hence the difference in the scattering power between water and PMMA (relative difference about 5 %) [48] could generate discrepancies in the predicted beam size smaller than 30 μm.

Another source of uncertainty for the model, which is difficult to quantify, lies within the normalization of the IDD curve to depth $z = 0$. The IDD was measured in water down to a minimum reachable depth of about 7 mm. The extrapolation of the experimental curve to depth $z = 0$ was done by means of a second-order polynomial fit. This choice was arbitrary but required to correlate the dose at a certain depth z to the fluence of primary protons at the phantom surface. In practice, a normalization to a depth z larger than the build-up region would be preferable, but it would require knowledge of the particle fluence at that specific depth.

In addition, according to ICRU Report 90 [49], the proton stopping power to water has a relative standard uncertainty of 1–3 %.

The agreement between FC-based calculated dose and dose measured with ionization chambers have been discussed in several works [8,21,50], and it is expected to depend on the design of the specific FC. Up to 6 % difference between FC and measured dose are reported in literature. In our pencil beam model, we have taken into account that the dose estimated with the PSI FC can be as much as (3±1) % lower than that measured with the ion-chamber, based on previous findings from Goma et al. [41] and Winterhalter et al. [51].

The Monitor 1 chamber was calibrated in terms of MU/p against the FC up to UHDR. The monitor showed significant recombination effects above 20 nA proton current, but the measured calibration curve demonstrated to be robust over time. The proposed method could represent a fast and reliable alternative which does not require modifications to the IC design or interventions on the operating parameters (e.g. chamber bias). As already mentioned in section 3.2, the delivered charge during the experiments with biological samples – controlled by Monitor 1 and verified by the FC – was always within ±1 % of the expected one, after applying daily corrections on the calibration according to daily reading of the FC.

An efficiency drop >30 % was also observed for the PTW TM7862 transmission chamber in the most challenging conditions (high beam current, small beam size). The characterization of the chamber was also

used to show how the collection efficiency is mainly dependent of the maximum current density, rather than on the average proton current.

With the presented irradiation setup, we could also test the dose rate dependence of different field detectors using the FC as reference. The PTW microDiamond showed about 1 % drop in sensitivity already at 10 Gy/s, and an additional 1 % decrease between 10 Gy/s and 2220 Gy/s. Potential effects due to misalignment of the beam vs microDiamond were excluded as the actual spot position for each delivery was measured on-line with the CCD-system. Measured fluctuations of the beam position were of the order of ±75 μm, which would results in variations in the measured dose <0.2 %.

It is currently under planning to explore even higher dose rates to verify if the microDiamond response settles to a certain 'saturation level'. Indeed this is what has been observed for UHDR pulsed electron beams [17], while Patriarca et al. [9] have recently reported no dose rate effects within the 3 % experimental uncertainty up to 80 Gy/s.

Similar sensitivity change as seen for the microDiamond – but with opposite sign – was found for the Gd_dO_2S:Tb scintillating screen. The increase of the scintillating efficiency at high dose rates was an unpredicted effect. That needs to be further investigated and verified. Possible secondary effects affecting the FC reading at different dose rates in the order of few percent are also to be considered. Favaudon et al. [35] tested a commercial device based on an inorganic scintillator for electron beams relative dosimetry in the ($0.4–3.5\times10^6$) Gy/s range with good results. Kanouta et al. [34] made use of small volume inorganic scintillators to measure the time structure of PBS proton deliveries up to 92.5 Gy/s, but a dose rate response characterization was not in the scope of their work. Our data show that the sensitivity change of Gd_dO_2S:Tb crystals is limited to a maximum of 3 % in the investigated range.

EBT3 Gafchromic™ films are one of the preferred choice for dosimetry in UHDR regimes. Jaccard et al. [28] verified the usability of EBT3 films for reference dosimetry in electron beams in the 7×10^3 to 8×10^6 Gy/s with accuracy of 4 % (k=2). Buonanno et al. [52] irradiated EBT3 films up to 1 kGy/s in a 4.5 MeV proton beam and no dependence on the mean dose rate was reported. Our results confirm that, within the measurement uncertainty of 2.4 % (k=1), the response of EBT3 films is not affected by dose rate in UHDR proton beams up to 9 kGy/s. However, a closer look at the data (Fig. 9a) might reveal an increase of sensitivity with dose rate similar to the one observed with the CCD-system, concealed by the measurement reproducibility. If demonstrated, this could be consistent with the recent findings by Villoing et al. [30]: in their work, they report an increase of the netOD for dose rates >1500 Gy/s and doses >10 Gy. Indeed, the data presented in Fig. 9a are measured at different dose levels in the (4–16) Gy range, with higher doses typically delivered at higher dose rates.

The beam size fluctuations described earlier (e.g. Fig. 10) between different measuring session, during the same session and for different dose rates affects the accuracy and reproducibility of the delivered dose when narrow single pencil beams are used to perform pre-clinical experiments. As such on-line measurements of the beam size of each delivered pencil beam is advisable in order to record, validate and eventually correct the actual delivered dose to biological samples or to detectors being investigated. We have shown that 2D detectors such as EBT3 films and scintillating CCD-systems could be employed for this purpose.

5. Conclusions

In this study, we have characterized an experimental setup that is being used for pre-clinical FLASH experiments in proton beams, and explored the challenges of reference dosimetry in millimetre-small UHDR proton pencil beams. A pencil beam dose model based on proton currents measured with a Faraday cup was implemented and validated through independent dose measurements. The dose measurements were performed with both passive detectors (EBT3 Gafchromic™ films, Al_2O_3:C OSLDs) and an active detector (PTW microDiamond 60019). Ion-recombination in air-vented ion chambers was characterized as a function of dose rate by means of the Faraday cup. A decrease in the collection efficiency >30 % was measured at the maximum proton current density for the PTW transmission chamber TM7862.

Limited sensitivity changes as function of dose rate were found for the PTW microDiamond, EBT3 Gafchromic™ films and the Gd_dO_2S:Tb scintillator. Further analysis are required to verify these results. Given its performance and its versatility, we believe the microDiamond is a reliable and practical alternative to passive detectors for dosimetry in UHDR proton beams. It shows the advantages of small-volume ionization chambers (e.g. energy independence) combined with a small dose rate dependence up to 2.2 kGy/s in quasi-continuous proton beams.

Declaration of Competing Interest

The authors declare that they have no known competing financial interests or personal relationships that could have appeared to influence the work reported in this paper.

Acknowledgements

The authors would like to thank Benno Rohrer and Martina Egloff for the valuable support in collecting the experimental data.

Disclosures

K. P. Nesteruk at the time of submission holds a research position at MGH. This study was conducted prior to that, when K. P. Nesteruk was a postdoc researcher at PSI. This work is partially funded by the Swiss National Science Foundation (grant No. 190663).

References

[1] Favaudon V, Caplier L, Monceau V, Pouzoulet F, Sayarath M, Fouillade C, et al. Ultrahigh dose-rate FLASH irradiation increases the differential response between normal and tumor tissue in mice. Sci Transl Med 2014;6(245). https://doi.org/10.1126/scitranslmed.3008973.

[2] Vozenin, M.C., et al., *The Advantage of FLASH Radiotherapy Confirmed in Mini-pig and Cat-cancer Patients.* Clin Cancer Res, 2019. **25**(1): p. 35-42.DOI: 10.1158/1078-0432.CCR-17-3375.

[3] Vozenin MC, Hendry JH, Limoli CL. Biological Benefits of Ultra-high Dose Rate FLASH Radiotherapy: Sleeping Beauty Awoken. Clin Oncol (R Coll Radiol) 2019;31(7):407–15. https://doi.org/10.1016/j.clon.2019.04.001.

[4] Levy K, Natarajan S, Wang J, Chow S, Eggold JT, Loo PE, et al. Abdominal FLASH irradiation reduces radiation-induced gastrointestinal toxicity for the treatment of ovarian cancer in mice. Sci Rep 2020;10(1). https://doi.org/10.1038/s41598-020-78017-7.

[5] Jaccard M, Durán MT, Petersson K, Germond J-F, Liger P, Vozenin M-C, et al. High dose-per-pulse electron beam dosimetry: Commissioning of the Oriatron eRT6 prototype linear accelerator for preclinical use. Med Phys 2018;45(2):863–74.

[6] Lempart M, Blad B, Adrian G, Bäck S, Knöös T, Ceberg C, et al. Modifying a clinical linear accelerator for delivery of ultra-high dose rate irradiation. Radiother Oncol 2019;139:40–5.

[7] Montay-Gruel P, Bouchet A, Jaccard M, Patin D, Serduc R, Aim W, et al. X-rays can trigger the FLASH effect: Ultra-high dose-rate synchrotron light source prevents normal brain injury after whole brain irradiation in mice. Radiother Oncol 2018;129(3):582–8.

[8] Diffenderfer ES, et al. Design, Implementation, and in Vivo Validation of a Novel Proton FLASH Radiation Therapy System. Int J Radiat Oncol Biol Phys 2020;106(2):440–8. https://doi.org/10.1016/j.ijrobp.2019.10.049.

[9] Patriarca A, Fouillade C, Auger M, Martin F, Pouzoulet F, Nauraye C, et al. Experimental Set-up for FLASH Proton Irradiation of Small Animals Using a Clinical System. Int J Radiat Oncol Biol Phys 2018;102(3):619–26.

[10] Weber UA, Scifoni E, Durante M. FLASH radiotherapy with carbon ion beams. Med Phys 2022;49(3):1974–92. https://doi.org/10.1002/mp.15135.

[11] Beyreuther E, Brand M, Hans S, Hideghéty K, Karsch L, Leßmann E, et al. Feasibility of proton FLASH effect tested by zebrafish embryo irradiation. Radiother Oncol 2019;139:46–50.

[12] Jolly S, Owen H, Schippers M, Welsch C. Technical challenges for FLASH proton therapy. Phys Med 2020;78:71–82.

[13] Schüller A, Heinrich S, Fouillade C, Subiel A, De Marzi L, Romano F, et al. The European Joint Research Project UHDpulse - Metrology for advanced radiotherapy using particle beams with ultra-high pulse dose rates. Phys Med 2020;80:134–50.

[14] Romano F, Bailat C, Jorge PG, Lerch MLF, Darafsheh A. Ultra-high dose rate dosimetry: Challenges and opportunities for FLASH radiation therapy. Med Phys 2022;49(7):4912–32.
[15] Subiel A, Moskvin V, Welsh GH, Cipiccia S, Reboredo D, DesRosiers C, et al. Challenges of dosimetry of ultra-short pulsed very high energy electron beams. Phys Med 2017;42:327–31.
[16] Petersson K, Jaccard M, Germond J-F, Buchillier T, Bochud F, Bourhis J, et al. High dose-per-pulse electron beam dosimetry - A model to correct for the ion recombination in the Advanced Markus ionization chamber. Med Phys 2017;44(3):1157–67.
[17] Kranzer R, Schüller A, Bourgouin A, Hackel T, Poppinga D, Lapp M, et al. Response of diamond detectors in ultra-high dose-per-pulse electron beams for dosimetry at FLASH radiotherapy. Phys Med Biol 2022;67(7):075002.
[18] Gómez F, Gonzalez-Castaño DM, Fernández NG, Pardo-Montero J, Schüller A, Gasparini A, et al. Development of an ultra-thin parallel plate ionization chamber for dosimetry in FLASH radiotherapy. Med Phys 2022;49(7):4705–14.
[19] Di Martino F, Del Sarto D, Giuseppina Bisogni M, Capaccioli S, Galante F, Gasperini A, et al. A new solution for UHDP and UHDR (Flash) measurements: Theory and conceptual design of ALLS chamber. Phys Med 2022;102:9–18.
[20] Marinelli M, Felici G, Galante F, Gasparini A, Giuliano L, Heinrich S, et al. Design, realization, and characterization of a novel diamond detector prototype for FLASH radiotherapy dosimetry. Med Phys 2022;49(3):1902–10.
[21] Winterhalter C, Togno M, Nesteruk KP, Emert F, Psoroulas S, Vidal M, et al. Faraday cup for commissioning and quality assurance for proton pencil beam scanning beams at conventional and ultra-high dose rates. Phys Med Biol 2021;66(12):124001.
[22] Darafsheh A, Hao Y, Zwart T, Wagner M, Catanzano D, Williamson JF, et al. Feasibility of proton FLASH irradiation using a synchrocyclotron for preclinical studies. Med Phys 2020;47(9):4348–55.
[23] Di Venanzio C, Marinelli M, Tonnetti A, Verona-Rinati G, Falco MD, Pimpinella M, et al. Characterization of a microDiamond detector in high-dose-per-pulse electron beams for intra operative radiation therapy. Phys Med 2015;31(8):897–902.
[24] Gomà C, Marinelli M, Safai S, Verona-Rinati G, Würfel J. The role of a microDiamond detector in the dosimetry of proton pencil beams. Z Med Phys 2016;26(1):88–94.
[25] Mandapaka AK, Ghebremedhin A, Patyal B, Marinelli M, Prestopino G, Verona C, et al. Evaluation of the dosimetric properties of a synthetic single crystal diamond detector in high energy clinical proton beams. Med Phys 2013;40(12):121702.
[26] Marinelli M, Pompili F, Prestopino G, Verona C, Verona-Rinati G, Cirrone GAP, et al. Dosimetric characterization of a synthetic single crystal diamond detector in a clinical 62 MeV ocular therapy proton beam. Nuclear Instruments & Methods in Physics Research Section a-Accelerators Spectrometers Detectors and Associated Equipment 2014;767:310–7.
[27] Marsolat F, De Marzi L, Patriarca A, Nauraye C, Moignier C, Pomorski M, et al. Dosimetric characteristics of four PTW microDiamond detectors in high-energy proton beams. Phys Med Biol 2016;61(17):6413–29.
[28] Jaccard M, Petersson K, Buchillier T, Germond J-F, Durán MT, Vozenin M-C, et al. High dose-per-pulse electron beam dosimetry: Usability and dose-rate independence of EBT3 Gafchromic films. Med Phys 2017;44(2):725–35.
[29] Jorge PG, Jaccard M, Petersson K, Gondré M, Durán MT, Desorgher L, et al. Dosimetric and preparation procedures for irradiating biological models with pulsed electron beam at ultra-high dose-rate. Radiother Oncol 2019;139:34–9.
[30] Villoing D, Koumeir C, Bongrand A, Guertin A, Haddad F, Métivier V, et al. Technical note: Proton beam dosimetry at ultra-high dose rates (FLASH): Evaluation of GAFchromic (EBT3, EBT-XD) and OrthoChromic (OC-1) film performances. Med Phys 2022;49(4):2732–45.
[31] Carrasco P, Jornet N, Jordi O, Lizondo M, Latorre-Musoll A, Eudaldo T, et al. Characterization of the Exradin W1 scintillator for use in radiotherapy. Med Phys 2015;42(1):297–304.
[32] Russo S, Mirandola A, Molinelli S, Mastella E, Vai A, Magro G, et al. Characterization of a commercial scintillation detector for 2-D dosimetry in scanned proton and carbon ion beams. Phys Med 2017;34:48–54.
[33] Safai S, Lin S, Pedroni E. Development of an inorganic scintillating mixture for proton beam verification dosimetry. Phys Med Biol 2004;49(19):4637–55. https://doi.org/10.1088/0031-9155/49/19/013.
[34] Kanouta E, Johansen JG, Kertzscher G, Sitarz MK, Sørensen BS, Poulsen PR. Time structure of pencil beam scanning proton FLASH beams measured with scintillator detectors and compared with log files. Med Phys 2022;49(3):1932–43.
[35] Favaudon V, Lentz J-M, Heinrich S, Patriarca A, de Marzi L, Fouillade C, et al. Time-resolved dosimetry of pulsed electron beams in very high dose-rate, FLASH irradiation for radiotherapy preclinical studies. Nuclear Instruments & Methods in Physics Research Section a-Accelerators Spectrometers Detectors and Associated Equipment 2019;944:162537.
[36] Christensen JB, Togno M, Nesteruk KP, Psoroulas S, Meer D, Weber DC, et al. Al2O3: C optically stimulated luminescence dosimeters (OSLDs) for ultra-high dose rate proton dosimetry. Phys Med Biol 2021;66(8):085003.
[37] Pedroni E, Bacher R, Blattmann H, Böhringer T, Coray A, Lomax A, et al. The 200-MeV proton therapy project at the Paul Scherrer Institute: conceptual design and practical realization. Med Phys 1995;22(1):37–53.
[38] Nesteruk KP, Togno M, Grossmann M, Lomax AJ, Weber DC, Schippers JM, et al. Commissioning of a clinical pencil beam scanning proton therapy unit for ultra-high dose rates (FLASH). Med Phys 2021;48(7):4017–26.
[39] Lin S, Boehringer T, Coray A, Grossmann M, Pedroni E. More than 10 years experience of beam monitoring with the Gantry 1 spot scanning proton therapy facility at PSI. Med Phys 2009;36(11):5331–40.
[40] Kacem H, Psoroulas S, Boivin G, Folkerts M, Grilj V, Lomax T, et al. Comparing radiolytic production of H2O2 and development of Zebrafish embryos after ultra high dose rate exposure with electron and transmission proton beams. Radiother Oncol 2022;175:197–202.
[41] Gomà C, Lorentini S, Meer D, Safai S. Proton beam monitor chamber calibration. Phys Med Biol 2014;59(17):4961–71.
[42] Safai S, Bortfeld T, Engelsman M. Comparison between the lateral penumbra of a collimated double-scattered beam and uncollimated scanning beam in proton radiotherapy. Phys Med Biol 2008;53(6):1729–50. https://doi.org/10.1088/0031-9155/53/6/016.
[43] Pedroni E, Scheib S, Böhringer T, Coray A, Grossmann M, Lin S, et al. Experimental characterization and physical modelling of the dose distribution of scanned proton pencil beams. Phys Med Biol 2005;50(3):541–61.
[44] Lynch GR, Dahl OI. Approximations to Multiple Coulomb Scattering. Nuclear Instruments & Methods in Physics Research Section B-Beam Interactions with Materials and Atoms 1991;58(1):6–10. https://doi.org/10.1016/0168-583x(91)95671-Y.
[45] Boag, J.W. and T. Wilson, *The Saturation Curve at High Ionization Intensity.* British Journal of Applied Physics, 1952. **3**(Jul): p. 222-229.DOI: Doi 10.1088/0508-3443/3/7/305.
[46] Devic S, Seuntjens J, Sham E, Podgorsak EB, Schmidtlein CR, Kirov AS, et al. Precise radiochromic film dosimetry using a flat-bed document scanner. Med Phys 2005;32(7Part1):2245–53.
[47] Christensen JB, Togno M, Bossin L, Pakari OV, Safai S, Yukihara EG. Improved simultaneous LET and dose measurements in proton therapy. Sci Rep 2022;12(1). https://doi.org/10.1038/s41598-022-10575-4.
[48] Safai S. Development of a dosimetric phantom with 400 pointlike scintillators coupled to optical light guides for 3D verification dosimetry for scanned proton beam. ETH Zürich; 2005.
[49] Seltzer, S.M., et al., *Key data for ionizing-radiation dosimetry: measurement standards and applications, ICRU Report 90.* 2016.
[50] Cambria R, Hérault J, Brassart N, Silari M, Chauvel P. Proton beam dosimetry: a comparison between the Faraday cup and an ionization chamber. Phys Med Biol 1997;42(6):1185–96.
[51] Winterhalter C, Fura E, Tian Y, Aitkenhead A, Bolsi A, Dieterle M, et al. Validating a Monte Carlo approach to absolute dose quality assurance for proton pencil beam scanning. Phys Med Biol 2018;63(17):175001.
[52] Buonanno M, Grilj V, Brenner DJ. Biological effects in normal cells exposed to FLASH dose rate protons. Radiother Oncol 2019;139:51–5. https://doi.org/10.1016/j.radonc.2019.02.009.